Acta Geotechnica
https://doi.org/10.1007/s11440-025-02735-3

RESEARCH PAPER

# Impact of reconstitution on the hydro-mechanical behaviour of Opalinus clay shale

Florian Christ[1] · Wolfgang Lieske[2] · Arash Alimardani Lavasan[3] · Eleanora Bakker[4] · Torsten Wichtmann[1]

Received: 7 January 2025 / Accepted: 21 July 2025


**Abstract**
This study investigates the impact of clay shale reconstitution on its hydro-mechanical behaviour, using grain size distribution as a key parameter to assess the degree of sample preparation. This topic is of practical relevance, as the characterisation of fine-grained soils often relies on their intrinsic properties, typically measured after reconstitution. While fine-grained soils that can be homogenised with minimal mechanical effort follow a fairly uniform preparation process, this is not the case for materials requiring initial pulverisation. To address this, three batches of remoulded Opalinus Clay samples (fine, medium, and coarse) were prepared. Their hydration curves, swelling pressure, and compressibility behaviour were analysed. Additional classification tests, pore size distribution measurements, and X-ray diffraction (XRD) analyses were performed to support physical characterisation. XRD revealed no preferential breakage of specific clay minerals or segregation of grain sizes. Test results indicated that preserved bonding in coarser grains acts as an additional attractive force, limiting hydration potential and reducing water adsorption. In contrast, finer materials showed higher hydration and swelling pressure due to increased surface area. While compressibility behaviour remained similar across samples at high stress, coarse-grained samples exhibited overconsolidated behaviour at low stresses, attributable to the structural integrity of larger grains.

**Keywords** Clay · Hydro-mechanical behaviour · Reconstitution · Shale · Soil structure · Swelling

## 1 Introduction

The hydro-mechanical behaviour of clays is governed by its structure, as well as the mineralogical composition. The term structure is generally understood as the combined effect of fabric and bonding, where the fabric describes the specific arrangement of soil constitutes and the bonding refers to frictionless connections between particles [6, 29]. The occurrence of these features depends on mineralogical composition, deposition, and geological history and might therefore significantly differ for a given mineralogical composition.

Effects that arise from structure and those related to intrinsic properties are often distinguished by assessing the soil behaviour in an undisturbed and in a specifically disturbed state, respectively [5, 6, 20, 26]. In [5] defines the intrinsic properties of a soil as those retained after thorough mixing at a water content above the liquid limit, a process known as reconstitution. This mechanical treatment partially destroys the bonding and removes the effects resulting from the geological history (e.g., effects from overconsolidation). To this end, it is apparent that the classification of cohesive soils is derived from the intrinsic

✉ Florian Christ
Florian.christ@rub.de

[1] Chair of soil mechanics, foundation engineering and environmental geotechnics, Ruhr-Universität Bochum, Building IC 5/101, Universitätsstraße 150, 44780 Bochum, Germany

[2] Local Authority for Soil Protection, Water and Harbours, Department of Environment and Urbanism, Herne, Germany

[3] Department of Engineering, Faculty of Science, Technology and Medicine, University of Luxembourg, Luxembourg, Luxembourg

[4] Institute of Concrete Structures and Building Materials (IMB-MPA-CMM), Karlsruhe Institute of Technology, Karlsruhe, Germany

Published online: 16 August 2025

soil properties, as the soil is reconstituted as part of the liquid limit determination procedure.

According to the terminology of structural units of a clay, a single clay layer consists of tetrahedral and octahedral sheets. For example held together by interlayer cations, these layers form a particle while several stacked particles shape an aggregate. In this context, the inter aggregate pores define the macroporosity, whereas intra-aggregate pores constitute the microporosity [9, 33, 37]. The size of aggregates is actually not limited; however, the term grain is used in the following for very large agglomerates of aggregates to avoid confusion. These grains consist of a large number of particles which are cemented by post sedimentation processes and thus do not correspond to the aggregate structure formed during sedimentation.

The smallest relevant units of soils, typically aggregates, are not fully destroyed during reconstitution [6, 15]. As a result, intrinsic soil properties depend not only on mineralogical composition but also on the internal structure of these aggregates [26]. If aggregates are disrupted by physical or chemical processes, the intrinsic properties of the soil degrade as well [15, 26]. This makes it essential to define which properties should be considered intrinsic, particularly for soils that cannot be reconstituted by simple mechanical stirring, such as highly overconsolidated (OC) structured clays. These clays, often found in a compacted state with significant bonding [17], are nevertheless commonly characterised in the literature by their liquid limits [8, 10, 34, 37].

A prominent example of such material is Opalinus Clay (OPA), a Jurassic-age marine claystone with partial structural bonding due to diagenetic processes [14]. OPA has been intensively studied in the context of deep geological repositories for radioactive waste in Switzerland. Research has covered its mechanical, hydro-mechanical, and thermo-hydro-mechanical behaviour [1, 7, 36, 44, 45], gas transport properties [19, 27, 42], and its chemical and biological characteristics [4, 25, 30]. Remoulded OPA has also been used to investigate basic material behaviour and the effects of diagenesis on structure and texture [7, 14, 16, 32]. The reconstitution process, which involves the merging of material from drill cores over a specific length, serves to mitigate the impact of natural local inhomogeneities.

From an engineering perspective, identifying intrinsic properties is vital for evaluating the in situ condition of structured soils. Furthermore, reconstituted clay shales are gaining importance due to their proposed use, often mixed with bentonite, as backfill and buffer materials in nuclear waste repositories [38, 47, 48]. Reconstituted clay shales are also useful for studying hydro-mechanical processes in the excavation damaged zone (EDZ), which forms during mechanised tunnelling [2, 43, 46]. In the EDZ, the material becomes disturbed, not as fine powder, but as a fragmented mass where cracks and joints dominate, resulting in a mix of disrupted rock and intact grains near the tunnel. This reconstituted behaviour defines the limit state of the disturbed material, contrasting with that of the intact host rock.

Above mentioned experimental studies on reconstituted clay shales have been conducted on a single given grain size distribution while its essential influence on the results has not been explicitly addressed. This raises the question of which properties are intrinsic and which can be influenced by modifying the grinding process and thus, are remnants of its structure. The only previous investigation into the influence of the particle size distribution of a crushed clay shale on the hydro-mechanical behaviour was conducted by [39]. However, in that study, the samples were analysed in a compacted state within an oedometer device and subjected to a variety of loading–unloading cycles, as well as water flooding tests. In contrast, the present study places a greater emphasis on the swelling and hydration behaviour, employing a different test programme. The focus of this study is on hydration characteristics, and the results provide a new and unique dataset with regard to these points.

In this frame, the present study aims to investigate the influence of the grain size in the reconstituted OPA samples on their liquid limit, mineralogy, and hydro-mechanical behaviour. For this purpose, Opalinus clay was grinded and processed into different granulates or rather powders, which are examined with respect to the properties mentioned above. Moreover, a series of mineralogical analysis was conducted to detect whether certain minerals fracture preferentially, thus are unevenly distributed among different fractions ($< 20$ µm, 20–250 µm, and $> 250$ µm) within the three respective powders (fine, medium, and coarse).

## 2 Materials and methods

### 2.1 Opalinus powder

The Opalinus clay shale in this study was obtained from the new Belchen A2 highway tunnel tube between Basel and Lucerne in Northern Switzerland, where it crosses the Jura mountains [49]. The material can be assigned to the shaly facies exhibiting an average clay mineral content of 64.4 wt% [50]. Regarding its mineralogical composition, the studied OPA is quite similar to the shaly facies of the Mont Terri underground research laboratory (e.g., average of 66% clay minerals; [3]).

Two of the three studied grain size distributions were achieved with different settings of the used jaw crusher, 1.2 and 1.0 mm opening width at 850 rpm and 900 rpm (coarse and medium), respectively. The third grain size

distribution was prepared from a subsequent milling process in a vibration mill for 5 min (fine). The final grain size distributions were then determined with a combined sieving (above 0.25 mm) and laser diffraction analysis (below 0.25 mm). For the laser diffraction analysis, the powder was ultrasonically dispersed for one minute with isopropyl alcohol as dispersant. The resulting grain size distribution curves for the OPA powders are presented in Fig. 1, including points from sieving (s) with filled symbols and laser diffraction analysis (l) with hollow symbols. They are termed fine, medium, and coarse in the following. The characteristic parameters of the grain size distributions are summarised in Table 1.

## 2.2 Geotechnical and chemico-physical characterisation

For the geotechnical and chemico-physical characterisation of the materials, several tests were conducted. The cation exchange capacity (CEC) was determined with the Cu-Triethylenetetramine method [28], quantifying the exchangeable cations. Liquid and plastic limits were determined according to DIN EN ISO 17892-12:2022-08 [11], whereby the Casagrande method was used for the liquid limit. The water uptake capacity was measured using the Enslin-Neff apparatus, historically based on [13] and [31].

## 2.3 Hydraulic and mechanical testing

### 2.3.1 Hydration curves

To allow the determination of the hydration curves, approximately 5 g of each powder (dried at 60 °C) were stored in small plastic lids in desiccators above oversaturated salt solutions for a controlled relative humidity. Desiccators again were stored in a temperature-controlled room, resulting in a controlled atmosphere and suction. Used salt solutions contained LiCl, $MgCl_2$, NaCl, KCl, $KNO_3$, and $K_2SO_4$, resulting in theoretical suctions of around 286 MPa, 96 MPa, 37 MPa, 20 MPa, 10 MPa, and 4 MPa at 20 °C. The material was weighed regularly, and its suction was measured in a chilled mirror hygrometer. Upon reaching an equilibrium value, materials were transferred to the next desiccator with a lower suction. Therefore, samples were stepwise hydrated.

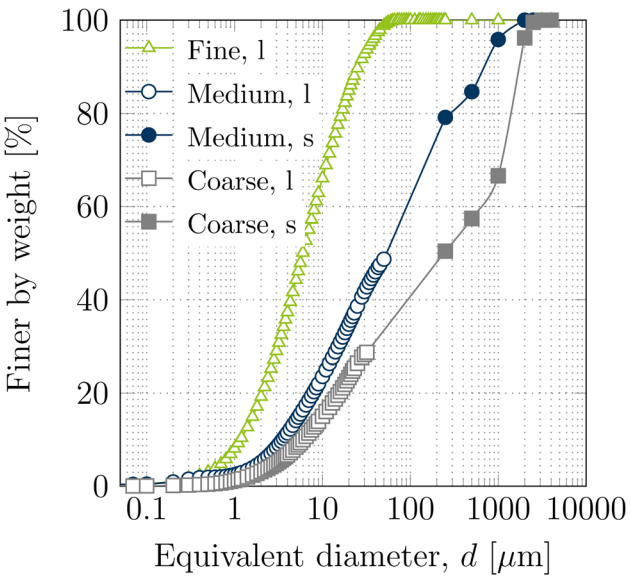


**Fig. 1** Grain size distributions of the three tested OPA powders

**Table 1** Parameters of the grain size distribution of the OPA powders used in present study

| | $d < 63\ \mu m$ [%] | $d < 2\ \mu m$ [%] | $d_{50}$ [μm] | $C_u$ [–] |
|---|---|---|---|---|
| Fine | 99.87 | 19.250 | 5.975 | 7.027 |
| Medium | 50.98 | 5.141 | 56.726 | 68.890 |
| Coarse | 29.60 | 3.117 | 249.789 | 106.094 |

### 2.3.2 Swelling pressure tests

Swelling pressure tests were conducted in swelling pressure cells at isochoric conditions. The target initial dry density for all three tests was chosen as 2.0 g/cm$^3$, resulting in the corresponding initial void ratio of 0.34. The initial water content was chosen to be the hygroscopic water content of the three powders, which were 2.61% for fine, 3.12% for medium and 3.81% for coarse. The material was statically compacted in the ring of the swelling pressure cells until a defined volume, and thus, target dry density was reached. The samples had a diameter of 5 cm and a height of 2 cm. The necessary compaction pressure was measured with a load cell installed at the hydraulic jack. Afterwards, the ring was transferred to the swelling pressure cell. One load cell is attached above and one beneath the sample to identify friction influences. For this simple setup, no considerable difference was found in the measured values of both cells. Nevertheless, the two values were averaged for the final swelling pressure presented in this study. The test set up is located in a temperature-controlled room (21 °C). Nevertheless, the cells are each additionally equipped with a temperature sensor. Due to the controlled temperature, which was confirmed by the sensors, temperature effects can be excluded in this study. Saturation was realised with a 0.5 m water column in a burette, attached to the porous stone at the bottom of the cell. Deionised water (DI-water) was used. An additional outlet at the bottom allows flushing of the porous stone.

Inlet and outlet at the top porous stone are open and allow the air in the sample to escape. Swelling process was assumed to be accomplished when an equilibrium in swelling pressure was observed.

#### 2.3.3 Oedometer tests

For the oedometer tests, materials were mixed with water corresponding to roughly 1.1–1.2 × its liquid limit resulting in a slurry. Afterwards, the slurry was placed in the oedometer ring without air inclusions. Samples measured 7 cm in diameter and 1.89 cm in height. The initial parameters obtained through this sample preparation method are summarised in Table 2.

Samples were stepwise loaded up to 1.2 MPa followed by an unloading back to 50 kPa using the same steps. The deformation was measured via linear variable differential transformers (LVDTs). Full saturation of the samples during the test was ensured by placing the setup in a tray filled with water.

### 2.4 Microstructural studies

#### 2.4.1 Mercury intrusion porosimetry

The pore size distribution of compacted OPA samples with fine and coarse grains having a dry density of $\rho_d$ = 2.0 g/cm$^3$ was determined via mercury intrusion porosimetry method before and after a swelling pressure test. For this purpose, the samples were broken in small pieces and rapidly frozen by means of liquid nitrogen. Afterwards, a freeze dryer was used to remove the water while preserving the microstructure. For mercury intrusion porosimetry, pressures up to 230 MPa were applied corresponding to an entrance pore size radius of about 3.3 nm.

### 2.5 Mineralogical studies

#### 2.5.1 Physical preparation

The > 250 µm fraction was separated by sieving the entire sample through a 250 µm sieve (between 50 and 75 g of starting material). A representative portion of 2–3 g of < 250 µm material was then obtained via repetitions of the coning and quartering method. This portion was then passed through a 20 µm sieve to separate the 250–20 and < 250 µm fractions. 1–2 g of the > 250 µm fraction was prepared for XRD analysis by hammer crushing, followed by milling for 10 min in a McCrone mill using corundum grinding elements and 20 cm3 ethanol. The resulting powder was passed through a 20 µm sieve, and the process was repeated until the whole sample passed through the sieve. McCrone milling in the same conditions was sufficient for the preparation of the 250–20 µm fraction. A sample of intact Opalinus clay was also prepared for XRD analysis via hammer crushing, hand milling in an agate mortar and pestle, and McCrone milling in order to investigate impacts of the grinding process on the deconsolidated Opalinus.

**Table 2** Initial parameters of the samples in the oedometer tests

| | | Fine | Medium | Coarse |
|---|---|---|---|---|
| Dry density, $\rho_d$ | [g/cm$^3$] | 1.171 | 1.361 | 1.465 |
| Void ratio, $e$ | [–] | 1.301 | 0.980 | 0.840 |
| Water content, $w_{init}$ | [%] | 48.9 | 34.9 | 36.44 |

#### 2.5.2 XRD analysis

Powder X-ray diffraction (pXRD) was used to analyse the mineralogy of the deconsolidated Opalinus clay samples. Oriented mounts prepared from 2 cm$^3$ aliquots of clay suspensions deposited on glass slides and allowed to air dry were used for identification of clay phases. A Bruker D8 Advance A25 diffractometer in Bragg–Brentano geometry (Bruker AXS GmbH, Karlsruhe, Germany) equipped with a LynxEye XE detector, a variable divergence slit (10 mm irradiated sample length), and 2.5° 2$\theta$ Soller slits (primary and secondary) was used. Patterns were recorded using Cu–Ka radiation from 3 to 80° 2$\theta$ (pXRD) or 3–50° 2$\theta$ (oriented mounts) using a step-size of 0.02°, counting time of 3 s per step, and sample rotation at 15 min$^{-1}$. XRD patterns of oriented slides were recorded under air-dried and ethylene glycol saturation conditions.

Oriented slides of clay fractions were prepared using the drip method from a portion of soil material dispersed with a sonicator in deionised water. XRD patterns of oriented slide preparations were recorded in air-dried and ethylene glycol solvated conditions. Phase content of pXRD samples was determined using Rietveld refinement via the Profex interface for BGMN software [12]. The R1 illite–smectite (IS-R1) structure from [40, 41] was used for modelling of interstratified illite–smectite phase content.

## 3 Results

The test program was designed in such a way that the influences of the grain size distribution on the hydration characteristics, the evolution of the swelling pressure and the compressibility can be analysed on the basis of mutually complementary individual tests. Therefore, in the following, the individual test results are described first,

**Table 3** Hygroscopic water content, cation exchange capacity, liquid limit, plastic limit, and plasticity index for all three materials

| | | Fine | Medium | Coarse |
|---|---|---|---|---|
| Hygroscopic water content, $w_{hyg}$ | [%] | 2.61 | 3.12 | 3.81 |
| Cation exchangce capacity, CEC | [meq/100 g] | 8.07 | 6.46 | 6.01 |
| Liquid limit, $w_l$ | [%] | 43.48 | 32.01 | 27.81 |
| Plastic limit, $w_p$ | [%] | 20.64 | 17.85 | 16.52 |
| Plasticity index, $I_p$ | [–] | 22.84 | 14.16 | 11.29 |

before they are discussed in Sect. 4 with respect to the previously mentioned topics.

### 3.1 Geotechnical and chemical-physical characterisation

The results obtained from geotechnical and chemophysical characterisation of the reconstituted powder samples with different grain sizes are summarised in Table 3. The hygroscopic water contents of the three different prepared powders show an increase with the grain size from fine (2.61%) over medium (3.12%) to coarse (3.81%). In contrast, the CEC decreases simultaneously from 8.07 over 6.46 to 6.01 meq/100 g. This fits with observations from [24], where the CEC increases linearly with increasing fraction $< 2$ µm.

According to Table 3, the liquid limit, plastic limit and plasticity index of OPA powders decrease with increasing the size of the grains. Transferring these values to the Casagrande diagram in Fig. 2, all three points are located on a line parallel to and above the A-line and are thus corresponding to a clay without organic matter. The coarse and medium coarse materials can be classified as clays with low plasticity (CL), whereas the fine material can be classified as a clay with medium plasticity (CI) with this method.

Figure 3 shows the water uptake capacity according to Enslin-Neff as the mean values obtained from duplicated tests for each grain size. As evident, the fine-grained material shows the highest rate of increase in water content at the beginning of the test and also the highest final water uptake capacity. According to Fig. 3, the least rate of water content uprise and lowest capacity of water uptake was observed for the coarse-grained samples while the results for the medium-sized grains lie between the fine and coarse results.

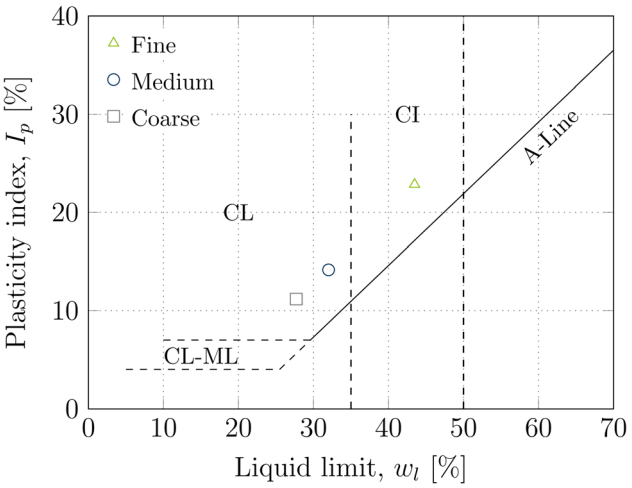


**Fig. 2** Plasticity chart for the remoulded OPA samples with different grain sizes

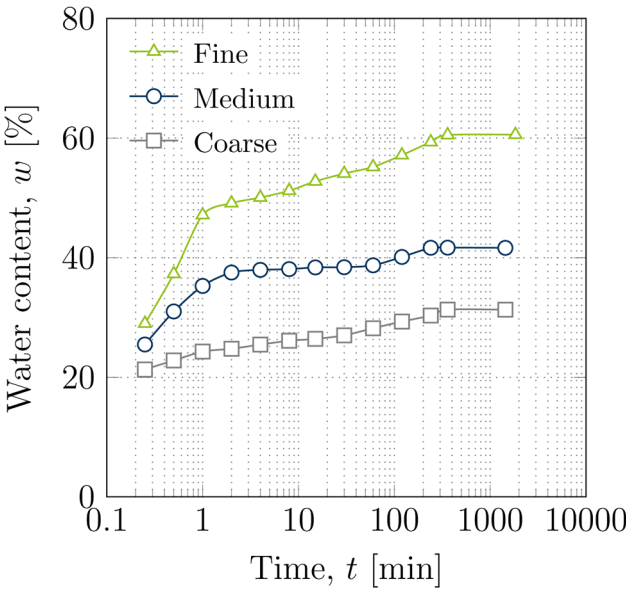


**Fig. 3** Variation of the water content with hydration time for the remoulded OPA samples with different grain sizes

### 3.2 Hydro-mechanical behaviour

#### 3.2.1 Hydration curves

At the beginning of the tests, all three materials are at 0% water content due to oven drying procedure. As shown in Fig. 4a, the drying stage is followed by the saturation of the OPA powder in six steps. The substantial increases in water content at particular times are attributed to the transfer of

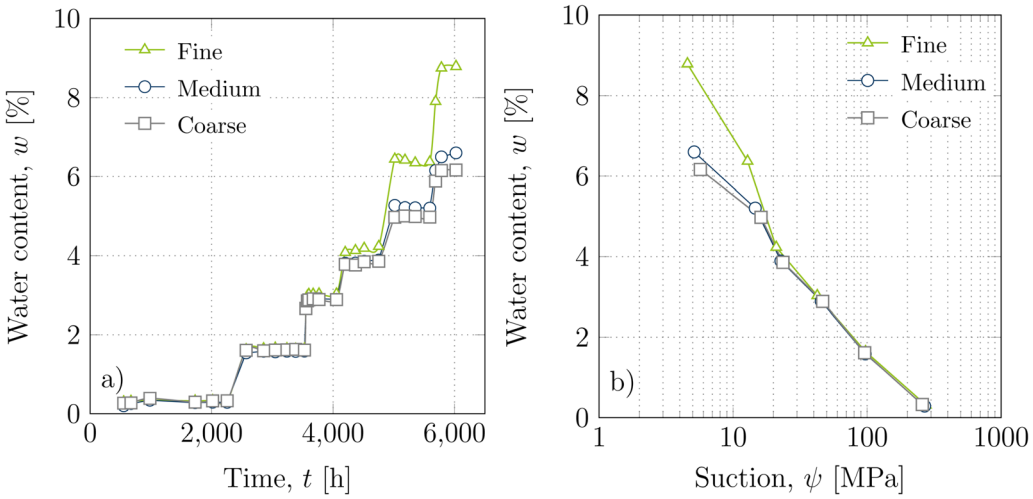


**Fig. 4** Water content over time (a) and over suction (b) for the three studied materials

the samples into a desiccator with a higher relative humidity. The initially relatively rapid increases and the subsequent constant levels of water content in Fig. 4a reflect the rapid adaptability of the water content of the samples to changing relative humidities. While the water contents of the different materials are at a similar level at the beginning of the test (for suctions between 286 and 96 MPa), they increasingly take on different water contents as the sample saturation increases and therefore suction decreases. In particular, the fine-grained sample is continuously deviating from the medium and coarse ones, showing a comparatively higher water content.

Figure 4b shows the hydration curves of the three materials as the equilibrium water content over the various suction levels on a semi-logarithmic scale. A linear increase in the water contents with decreasing suction for suctions higher than 20 MPa can be observed. In that suction range, the hydration curves are rather independent of grain size. However, a remarkable deviation between the hydration curves can be observed at suctions lower than 20 MPa, where the hydration curve of the samples with fine grains lies significantly above those for the medium and coarse ones.

#### 3.2.2 Swelling pressure tests

The swelling pressure development over time for the three materials is presented in Fig. 5a where dissimilarities in both the equilibrium swelling pressure and its evolution rate are observed. According to Fig. 5a, fine and medium-grained samples reach equilibrium swelling pressures of about 1820 and 640 kPa, respectively, in approximately 16 h, while the coarse sample exhibits an equilibrium swelling pressure of 430 kPa at about 8 h. In case of fine and medium-grained samples, the swelling pressure curve shows a fluctuation that consists of an approximately 10% drop in the swelling pressure curve at a certain pressure state (i.e., 1730 and 640 kPa, respectively, for fine and medium samples) prior to the equilibrium state. Figure 5a shows that the medium sample instantly reaches the equilibrium swelling pressure after the drop, whereas the fine sample reveals further swelling pressure build-up before reaching the equilibrium swelling pressure. However, such phenomenon was not observed for the coarse sample. Evidently, the equilibrium swelling pressure of the fine sample is significantly higher compared to the medium and coarse ones.

The compaction pressure required to produce the compacted samples is plotted versus the equilibrium swelling pressure in Fig. 5b. Obviously, when increasing the grain size in powder- compacted samples, lower compaction pressure is necessary to fabricate samples at a given dry density. In particular, a significantly higher compaction pressure of about 30 MPa was required to produce the sample with the dry density of 2 g/cm$^3$ from fine OPA grains, which is about three times higher than the compaction pressure needed for the coarse sample. According to Fig. 5b, the equilibrium swelling pressure increases linearly with the compaction pressure. This means that the compaction pressure needed to produce samples with identical dry density and the corresponding equilibrium swelling pressure both increase with decreasing grain size of OPA, while a linear relationship is observed between both pressures.

### 3.3 Compression behaviour

The results of the oedometer tests conducted on samples with different grain sizes are presented in Fig. 6. The compression and swelling indices obtained from these tests

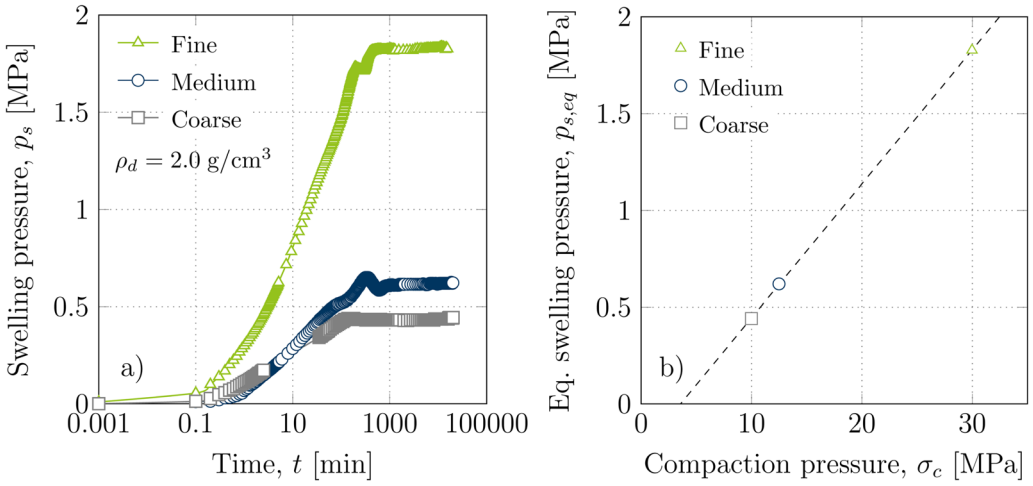


**Fig. 5** Swelling pressure of the three studied materials over time (a) and compared to the required compaction pressure for reaching a dry density of 2.0 g/cm$^3$ (b)

have been summarised in Table 4. According to Table 4, both compression and swelling indices ($\lambda$ and $\kappa$) increase with decreasing grain size. Figure 6 and Table 4 illustrate rather similar behaviour and parameters for the medium and coarse material. The intrinsic compression line (ICL) according to [5] in Fig. 6b is defined with the actual experimentally identified $e^*_{100}$ and $e^*_{1000}$ (void ratios on the ICL at vertical stresses of 100 and 1000 kPa, respectively) from Fig. 6a, according to Eq. 1. This results in one ICL for all three materials. In contrast, the three curves of the void index $I_v$ shown in Fig. 6b consider a normalisation with the liquid limits of the three materials, by determining the normalised void ratio at a vertical stress of 100 kPa $e^*_{100,el}$ and normalised compression index $C^*_{c,el}$ in accordance with empirical relationships as proposed in Eqs. 2 and 3 by [5]. This means that Eq. 1 was also used for these 3 curves, but with $e^*_{100,el}$ and $e^*_{1000,el}$ instead of experimental determined $e^*_{100}$ and $e^*_{1000}$. All materials meet the conditions for using these empirical equations, since their liquid limit lies between 25 and 160% and they are located above the A-Line in the plasticity chart.

$$I_v = \frac{e - e^*_{100}}{e^*_{100} - e^*_{1000}} \tag{1}$$

$$e^*_{100,el} = 0.109 + 0.679 e_l - 0.089 e_l^2 + 0.016 e_l^3 \tag{2}$$

$$C^*_{c,el} = 0.256 e_l - 0.04 = e^*_{100,el} - e^*_{1000,el} \tag{3}$$

where $e_l$ is the void ratio at the liquid limit and all parameters are dimensionless. Results for $e_l$, $e^*_{100,el}$, $e^*_{1000,el}$ and $C^*_{c,el}$ are summarised in Table 5. As shown in Fig. 6b, the curves of void index versus vertical stress for samples with distinct grain sizes lie above the experimentally determined ICL.

To determine the constrained modulus $M$ according to [21] as a secant modulus, Eq. 4 is employed and the corresponding results have been presented in Fig. 6c.

$$M = \frac{\Delta\sigma_1'}{\Delta\varepsilon} \tag{4}$$

where $\Delta\sigma_1'$ and $\Delta\varepsilon$ are the increments of vertical effective stress and strain, respectively. As evident in Fig. 6c, the constrained modulus for high stresses varies almost linearly with vertical stress. However, for smaller stresses, there is a typical deviation for diagenetic or preloaded material. The vertical load at which the material follows the linear curve decreases as the material becomes finer. Moreover, comparison of the results obtained from present experiments with those reported by [14] on remoulded OPA samples shows a good agreement. The OPA from a shallow depth (around 300 m) from Mont Terri used by [14] is similar in mineralogical composition and burial diagenesis to the material from the Belchen tunnel site used in this study. Results of intact OPA in the same study approach the best-fit line at significantly higher vertical stresses. Figure 6d shows the measured coefficient of consolidation ($c_v$) as an estimate for the hydraulic permeability of the investigated materials. As expected, the samples with finer grains exhibit lower coefficients of consolidation. Moreover, the coefficient of consolidation increases with vertical stress up to about 500 kPa while the opposite trend is observed at higher pressures.

The variation of experimentally determined $e^*_{100}$ and $C^*_c$ values versus void ratio at the liquid limit (el) obtained for the samples with different grain sizes in the present study is plotted in Fig. 7, along with the results of [14] showing a good agreement of both datasets. The dashed lines in Fig. 7, representing a fitting of the three

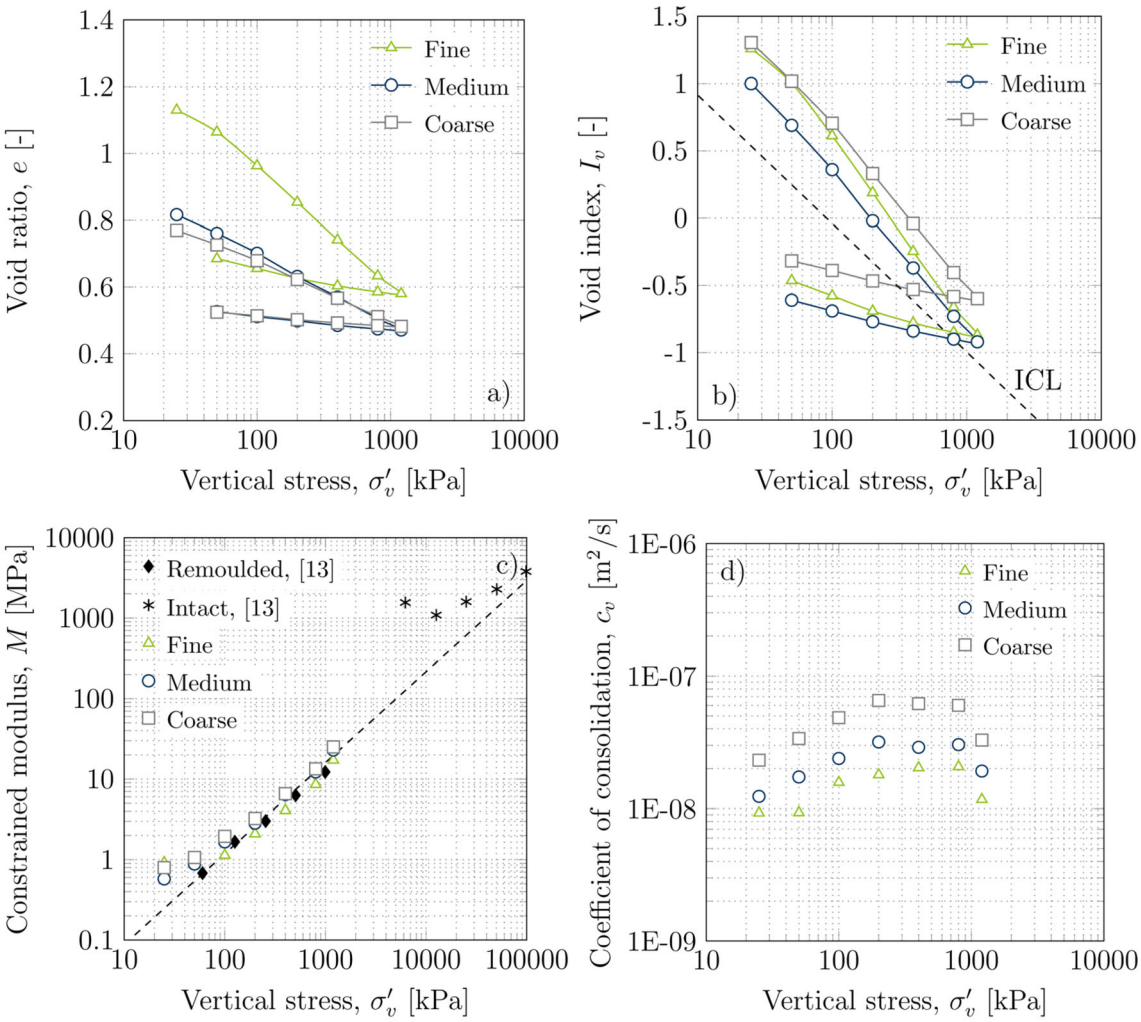


**Fig. 6** Oedometer test results: **a** void ratio $e$, **b** void index $I_v$, **c** constraint modulus $M$ and **d** coefficient of consolidation $c_v$ as function of vertical stress $\sigma'_v$

**Table 4** Compression and swelling index from oedometer tests on remoulded OPA samples with different grain sizes

| | | Fine | Medium | Coarse |
|---|---|---|---|---|
| $\Lambda$ | [–] | 0.152 | 0.091 | 0.077 |
| $K$ | [–] | 0.033 | 0.017 | 0.013 |

**Table 5** Theoretically calculated $e^*_{100,el}$, $e^*_{1000,el}$ und $C_c{}^*_{,el}$ according to equations from [5] depending on void ratio at liquid limit $e_l$

| | | Fine | Medium | Coarse |
|---|---|---|---|---|
| $e_l$ | [–] | 1.166 | 0.858 | 0.746 |
| $e^*_{100,el}$ | [–] | 0.805 | 0.636 | 0.572 |
| $e^*_{1000,el}$ | [–] | 0.547 | 0.457 | 0.421 |
| $C_c{}^*_{,el}$ | [–] | 0.258 | 0.858 | 0.151 |

experimental data points from the present study, lie somewhat above the regression lines according to [5].

### 3.4 Mineralogical analysis

The results of the pXRD analysis on the different subsamples are summarised in Table 6. Qualitative interpretation of XRD results revealed a mineral assemblage typical of Opalinus clay. No trace of gypsum was found, indicating no artificial alteration of the samples. Quantitative analysis reveals the main phases as IS-R1 (average content 25%), muscovite/illite (22%), quartz (16%), kaolinite (13%), calcite (7%), and minor phases as chlorite (5%), feldspars (plagioclase 4%; K-feldspar 2%), dolomite (3%), siderite (2%), pyrite (1%), and anatase and rutile (both < 1%). This composition is typical for the Opalinus shaly facies. The phase contents of the fractions taken from the fine, medium, and coarse samples were found to be

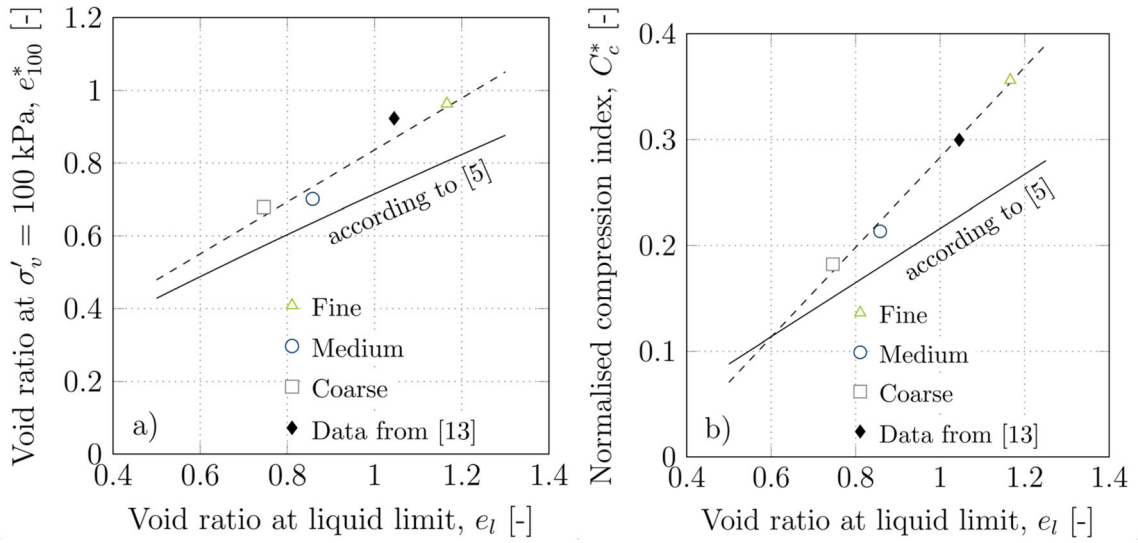


**Fig. 7** Void ratio on ICL at 100 kPa vertical stress (a) and intrinsic compression index (b) over void ratio at liquid limit for the three materials with different grain sizes

very similar to those of the intact sample, showing no evidence of amorphisation due to the grinding process. The largest variation in content between different samples was observed for the IS-R1 phase. A larger variation of the content of this phase is expected due to the difficulty in modelling clay phases. Furthermore, chlorite is slightly higher in the $f < 20$ µm sample, but the influence on the abundance of the other phases is small, as the difference is only + 3%. Such differences could be due to imperfect sample preparation, e.g., non-uniform crystallite size in the XRD sample due to grinding/sieving or preferential orientation in the pXRD sample. There is no systematic variation in mineralogy between the fine, medium, and coarse samples, nor between the > 250, 250–20, and < 20 µm size fractions. Their compositions are similar within the degree of accuracy of the methodology and indicated that grinding does not selectively impact certain mineral phases.

### 3.5 Microstructural analysis

The pore size distributions of fine and coarse compacted OPA samples are shown in Fig. 8 in terms of the pore size density function for the initially compacted state (initial) and after a swelling pressure test at constant volume conditions (swollen). The curves are typical for a double-porosity structure, with a first peak corresponding to the micropores (ultramicroporosity and microporosity summarised as micropores with $r < 50$ nm) and a second peak pertaining to the macropores (mesoporosity and macroporosity summarised as macropores with $r > 50$ nm). Evidently, no significant difference in the micropore regime of the coarse and fine samples in the initial state was observed. However, the macropore regimes of fine and coarse samples significantly differ in the initial state, with the coarse sample having larger macropores compared to the fine material. According to Fig. 8, the constant volume swelling of the samples affects the macropores in terms of the peak density (increased by swelling) and the size of the macropores (reduced by swelling) for both coarse and fine materials.

## 4 Discussion

### 4.1 Influence of the grain size on the hydration characteristics

The water content–suction relationship (Fig. 4b) reveals similar behaviour among all materials at suctions above 18 MPa, while distinct differences emerge below this threshold. Likewise, free water uptake (Fig. 3) strongly depends on the grain size of the remoulded OPA samples. Water retention in clayey soils is influenced by mineralogy and exchangeable cations (e.g., surface and cation hydration), as well as by fabric-related factors such as capillarity. According to [23], three regimes of water retention exist, increasing in suction: capillary water, adsorbed water, and tightly adsorbed water. The latter is primarily governed by cation–surface interactions and is closely linked to the cation exchange capacity (CEC) and specific surface area (SSA). At high suctions, where cation hydration dominates, the three tested materials exhibit comparable retention behaviour. Although CEC increases from coarse to fine fractions by approximately 33%, the absolute differences remain minor and insufficient to account for significant

**Table 6** Summary of the pXRD results for all tested subsamples

| Sample | IS-R1 [%] | Muscovite 2M1 [%] | Kaolinite 1A [%] | Chlorite (donbassite) [%] | Quartz [%] | Plagioclase (albite) [%] | K-feldspar (microcline) [%] | Calcite [%] | Ankerite [%] | Siderite [%] | Pyrite [%] | Anatase [%] | Rutile [%] |
|---|---|---|---|---|---|---|---|---|---|---|---|---|---|
| C > 250 | 24.9 | 21.5 | 13.1 | 4.9 | 16.3 | 3.4 | 2.1 | 6.9 | 2.6 | 1.7 | 1.1 | 0.8 | 0.7 |
| C 250–20 | 27.0 | 20.4 | 12.3 | 4.8 | 16.5 | 3.2 | 2.1 | 6.9 | 2.8 | 1.6 | 1.1 | 0.8 | 0.6 |
| C < 20 | 20.3 | 23.4 | 14.7 | 4.8 | 16.6 | 3.5 | 2.1 | 7.0 | 3.3 | 1.8 | 1.0 | 0.6 | 0.7 |
| M > 250 | 26.8 | 21.0 | 12.9 | 4.9 | 15.8 | 3.4 | 1.9 | 6.5 | 2.3 | 2.0 | 1.2 | 0.8 | 0.7 |
| M250-20 | 26.7 | 20.3 | 12.4 | 4.4 | 17.4 | 3.6 | 2.0 | 7.0 | 2.5 | 1.5 | 1.0 | 0.8 | 0.6 |
| M < 20 | 23.6 | 21.6 | 14.3 | 3.6 | 15.5 | 4.7 | 3.1 | 5.6 | 4.4 | 1.5 | 0.8 | 0.5 | 0.9 |
| F > 250 | 29.7 | 20.8 | 13.1 | 4.0 | 14.4 | 3.4 | 1.9 | 6.1 | 2.7 | 1.5 | 1.1 | 0.8 | 0.6 |
| F250-20 | 20.8 | 21.0 | 13.6 | 4.5 | 18.1 | 4.0 | 2.5 | 7.8 | 3.2 | 1.5 | 1.6 | 0.8 | 0.6 |
| F < 20 | 21.1 | 23.8 | 11.6 | 7.3 | 16.4 | 3.6 | 2.6 | 6.2 | 3.1 | 1.8 | 1.0 | 0.9 | 0.8 |
| Intact | 27.5 | 20.4 | 12.3 | 4.3 | 17.0 | 3.3 | 2.2 | 6.0 | 1.7 | 2.4 | 1.7 | 0.7 | 0.5 |
| Mean | 24.8 | 21.4 | 13.0 | 4.7 | 16.4 | 3.6 | 2.2 | 6.6 | 2.9 | 1.7 | 1.1 | 0.8 | 0.7 |

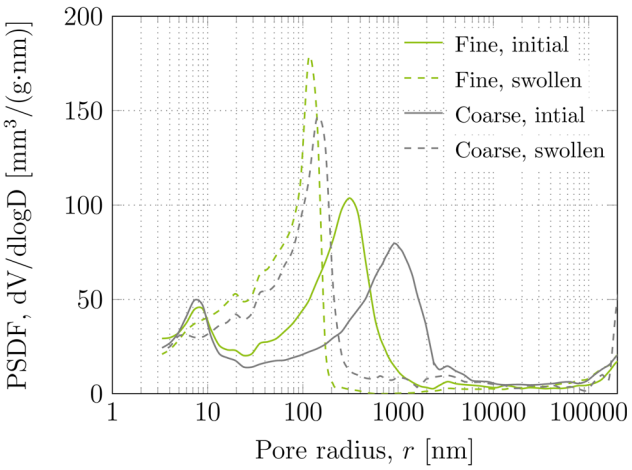


**Fig. 8** Pore size density functions of compacted fine and coarse OPA powder before and after a constant volume swelling pressure test

variation in water uptake. XRD analysis (Sect. 3.4) confirmed that grinding did not alter mineral composition or lead to selective fragmentation of clay minerals. Instead, grinding primarily affected particle structure, increasing the number of smaller grains by breaking interparticle bonds. This increase in surface area available for hydration explains the higher water uptake in finer-grained samples. While this finding contrasts with [35], who observed higher water absorption in bentonite granules compared to powder, their results can be attributed to the larger, more connected pore structure in the granules, which promotes greater water retention.

As the MIP data in Fig. 8 revealed, the grain size distribution does not affect the initial micropores of the compacted OPA samples. Unlike bentonite in granular form, Opalinus grains have a strong additional attractive force due to the rock forming clay mineral calcite that induces a bonding which is commonly observed in sedimentary rocks and also found in the present study (Table 3). Such a bonding phenomenon hinders the expansion of very dense grains. Additionally, the pore connection of clay shales has been observed in the literature to be poor [22]. Therefore, in the case of a finely ground clay rock, a lower stabilising effect of the bonding coincides with a larger free surface that elevates the hydration capacity.

## 4.2 Influence of the grain size on the evolution of swelling pressure

The mechanisms previously discussed in the context of the different hydration behaviours play also a crucial role with respect to the rate and potential of swelling pressure evolution. As demonstrated in Fig. 5, the absolute swelling pressure is significantly higher for the fine OPA sample.

This is consistent with the considerably higher adsorption of water by the assembly of fine grains. The difference in water absorption between the OPA powders with medium and coarse grains is less significant in the tests on water uptake capacity (Fig. 3) and on hydration characteristics (Fig. 4), which is also evident in a smaller absolute difference in their swelling pressures (Fig. 5). Again, the intrinsic bonding within the OPA grains acts as an additional attractive force that reduces the swelling potential. This force also explains why the fluctuation of the swelling pressure before reaching an equilibrium value is more pronounced in the fine and medium material than in the coarse one. The observed fluctuation can be attributed to a rearrangement of particles [18], which is reduced in the case of larger grains due to the intrinsic bonding that prevails in them. The coefficients of consolidation ($c_v$) obtained from the oedometer tests (Fig. 6d) indicated an increasing trend of higher hydraulic conductivities with coarser grain size distribution. This is the case because $M$ does not vary significantly for the three materials and shows the same tendency with grain size as $c_v$ (Fig. 6c). However, this trend is not reflected in the courses of the constant volume swelling pressure tests, where the swelling pressure of fine material showed the highest magnitude and rate of evolution. As mentioned before, the well-connected macropore structure in fine sample enables a quicker hydration while the lower bonding effect in the fine grains allows higher swelling pressure build-up. The lower free surface of coarse powder and the lesser local permeability of the grains compared with fine powder decelerates the water absorption process and swelling pressure evolution. This mechanism is evaded in the oedometer tests by installing the initial material as a slurry. Thus, the fine material forms a homogeneous sample with a low permeability. According to Fig. 5b, the required compaction pressure to reconstitute the sample to a target dry density of 2.0 g/cm$^2$ increases with decreasing the size of the grains. This is because the intact material has a dry density of around 2.3 g/cm$^2$ and the milled grains preserve a similar dry density. Accordingly, large grains with higher dry density than the target value require less compaction pressure as well as less volume of the initial material in powder form to produce the reconstituted sample. In general, the compacted sample from fine powder is much more homogeneous than that of the coarse powder. As a consequence, a linear correlation between compaction pressure and corresponding swelling pressure was observed.

### 4.3 Influence of the grain size on the compressibility

The oedometer test results as shown in Fig. 6a depicted considerable differences in the compression behaviour of the different materials. Moreover, a deviation in the initial state of the material that started from a water content above the liquid limit was seen. Assessment of the constrained modulus as shown in Fig. 6c indicated that all materials follow the same pattern at the high stress range. However, all remoulded OPA samples fabricated in this study showed an effect of overconsolidation or evidence of structure at low pressures that is illustrated as a deviation from the unique linear trend indicated by the dashed line. The fine material approaches the dashed line at lower stresses (approx. 100 kPa) while such transition is observed at a range of 200–300 kPa in case of coarse material. According to Fig. 6c, the very fine material tested by [14] already reaches the linear course at 60 kPa, which can be attributed to the sieving of the coarse material leading to the exclusion of any remaining structure from the samples. An approximation to the dashed line is also evident for the intact sample tested by [14]. It could therefore be concluded that all materials show a similar deformation behaviour in the normally consolidated state. Vice versa, despite the remoulding some of the reconstituted samples show overconsolidation effects preserved by the strong bonding.

If the void ratio versus vertical stress plot is normalised according to the void index concept of [5], as shown in Fig. 6b, all remoulded materials lie to the right of the intrinsic compression line, which intuitively indicates incomplete destructuring. However, considering the parameters $e^*_{100}$ and $C^*_c$ over $e_1$ in Fig. 7, that have been employed for the normalisation, a different aspect emerges. It appears that the correlation proposed by [5] fits best for the coarse material, while the fine and medium material as well as the material studied by [14] follow a different correlation (dashed line). Evidently, with increasing liquid limit (or decreasing the grain size), both $e^*_{100}$ and $C^*_c$ exceed the correlation suggested by [5]. This is in general agreement with the observation of [5] who stated deviations from his correlation for high and low liquid limits.

The interaggregate bonds in the materials investigated by Burland are rather weak, and as such, they can be destroyed by subjecting the material to mixing at a water content above the liquid limit. In the process of remoulding, the intra-aggregate bond remains intact, thereby preserving the overall fabric. Subsequent treatment, such as the drying of the material, which results in alterations to the structure, would no longer be an accurate reflection of the intrinsic properties. In the case of OPA, the material is not characterised by an aggregated structure, nor is it possible to remould it by mixing above the liquid limit. This difficulty in identifying the material's intrinsic properties is due to the aforementioned characteristics. Nevertheless, in order to analyse the influence of diagenesis on the mechanical properties of the material, it becomes apparent

that the most highly processed powder demonstrates the least influence of diagenesis. For instance, the constrained modulus demonstrates that the load with which the material follows an NC path decreases with the fineness.

## 5 Conclusions

This paper experimentally examined the influence of the grain size distribution on the hydro-mechanical behaviour and compressibility of reconstituted Opalinus clay shale (OPA). Three different batches of OPA powder (fine, medium, and coarse) were prepared, classified, and mineralogically analysed. Classification results showed clear trends from fine over medium to coarse material in all tests. The XRD investigations indicated that both, preferential breakage of specific clay minerals and amorphisation are negligible. Uneven segregation of minerals in tested subsamples does not occur. The materials were furthermore tested regarding their hydration, swelling, and compressibility behaviour. The results from the classification were taken into account in the discussion of the outcomes of the further experiments. Based on the results obtained in this study, the following concluding remarks could be drawn:

- The intrinsic bonding that remains in the larger grains of OPA in coarse material acts as an additional attractive force and counteracts the expansion upon hydration. Additionally, the larger free surface of finer material accelerates the hydration process and results in a generally higher water absorption capacity. This is in contrast to observations made with bentonite, where the large pore space of the granules favours water absorption (e.g., [35]).
- The differences in the hydration process of samples with different grain sizes are also reflected in the magnitude of the swelling pressure. The increased water adsorption capacity of fine material raises the swelling pressure, while the additional attractive force due to remaining bonding in the larger grains of coarse material reduces the swelling pressure.
- The similar constrained moduli from oedometric compression tests in the high stress regime for different grain sizes reveal the similar behaviour in the normally consolidated state. The remaining bonding of grains however resulted in obvious overconsolidation effects at lower stresses. The investigation revealed the weakest influence of these overconsolidation effects for the finest material. This influence was even less evident in a dataset of [14] where the material was sieved before testing, excluding coarse grains.

In conclusion, it can be stated that finer powders should be preferred for investigations on the intrinsic behaviour of ground clay shale, since effects of overconsolidation are still visible in the coarse powders. It was found that the coarse material could be sieved off in the preparation process, as this does not alter the mineralogical composition of the powder due to preferred crushing of certain clay minerals. The absence of compelling evidence for significant mineralogical influences suggests that these findings may also be applicable to other swellable clay shales.

The present study offers valuable insights for the future investigation of excavated material in the construction process of radioactive waste repositories for its suitability as backfilling and for dimensioning with regard to hydro-mechanical behaviour based on the fineness of grinding. It also raises awareness of the relevance of sample preparation procedure and explicitly the grain size distribution to hydro-mechanical behaviour. The hydro-mechanical behaviour of a specific grain size distribution is not necessarily characteristic of the material in general.

The data and findings obtained provide a basis for further investigations and have raised additional questions. It is suggested that further studies should be conducted on the following aspects: the influence of temperature (annual temperature cycles in transport tunnels or the decay heat of radioactive waste); and the influence of pore water chemistry (in situ water or bleeding water from grouting material). Corresponding studies have already been scheduled.

**Acknowledgements** The authors would like to gratefully acknowledge the financial support by the German Research Foundation (DFG) through the collaborative research centre (SFB 837), subproject A5, and Dr. Martin Ziegler (Department of Earth Sciences, ETH Zurich) for providing the studied Opalinus material. The drilling and sampling works were financed by the Swiss Federal Nuclear Safety Inspectorate (ENSI) in the frame of the STB (Sanierungstunnel Belchen) project. The laboratory work was supported by Natascha Kallerhoff.

**Funding** Open Access funding enabled and organized by Projekt DEAL.

**Data availability** The authors declare that the data supporting the findings of this study are available within the paper. Should any raw data files be needed in another format they are available from the corresponding author upon reasonable request.

## Declarations

**Conflict of interest** The authors declare no competing interests.

## References


1. Bossart P, Jaeggi D, Nussbaum C (2017) Experiments on thermo-hydro-mechanical behaviour of Opalinus Clay at Mont Terri rock laboratory, Switzerland. J Rock Mech Geotech Eng 9:502–510. https://doi.org/10.1016/j.jrmge.2016.11.014
2. Bossart P, Meier PM, Moeri A, Trick T, Mayor JC (2002) Geological and hydraulic characterisation of the excavation disturbed zone in the Opalinus Clay of the Mont Terri Rock Laboratory. Eng Geol 66(1–2):19–38. https://doi.org/10.1016/S00137952(01)00140-5
3. Bossart P, Thury M (2008). Project, programme 1996 to 2007 and results. Wabern: Reports of the Swiss Geological Survey no. 3
4. Boylan A, Perez-Mon C, Guillard L, Burzan N, Loreggian L, Maisch M, Kappler A, Byrne J, Bernier-Latmani R (2019) H2-fuelled microbial metabolism in Opalinus Clay. Appl Clay Sci 174:69–76. https://doi.org/10.1016/j.clay.2019.03.020
5. Burland JB (1990) On the compressibility and shear strength of natural clays. Geotech 40(3):329–378
6. Cotecchia F, Chandler RJ (2000) A general framework for the mechanical behaviour of clays. Geotech 50(4):431–447. https://doi.org/10.1680/geot.2000.50.4.431
7. Crisci E, Ferrari A, Giger SB, Laloui L (2019) Hydro-mechanical behaviour of shallow Opalinus Clay shale. Eng Geol 251:214–227. https://doi.org/10.1016/j.enggeo.2019.01.016
8. Dehandschutter B, Vandycke S, Sintubin M, Vandenberghe N, Wouters L (2004) Britlle fractures and ductile shear bands in argillaceous sediments: inferences from Oligocen Boom Clay (Belgium). J Struct Geol 27:1095–1112
9. Delage P, Marcial D, Cui YJ, Ruiz X (2006) Ageing effects in a compacted bentonite: a microstructure approach. Geotech 56(5):291–304. https://doi.org/10.1680/geot.2006.56.5.291
10. Deng YF, Tang AM, Cui YJ, Li XL (2011) Study on the hydraulic conductivity of Boom clay. Can Geotech J 48(10):1461–1470. https://doi.org/10.1139/t11-048
11. DIN EN ISO 17892-12:2022-08 (2022). Geotechnical investigation and testing - laboratory testing of soil - part 12: determination of liquid and plastic limits (ISO 17892-12:2018 + Amd 1:2021 + Amd 2:2022); German version EN ISO 17892-12:2018 + A1:2021 + A2:2022
12. Doebelin N, Kleeberg R (2015) Profex: a graphical user interface for the Rietveld refinement program BGMN. J Appl Crystallogr 48(5):1573–1580. https://doi.org/10.1107/S1600576715014685
13. Enslin O (1933) Über einen Apparat zur Messung der Flüssigkeitsaufnahme von quellbaren und porösen Stoffen und zur Charakterisierung der Benetzbarkeit. Die chemische Fabrik 13:147–148
14. Favero V, Ferrari A, Laloui L (2016) On the hydro-mechanical behaviour of remoulded and natural Opalinus Clay shale. Eng Geol 208(3):128–135. https://doi.org/10.1016/j.enggeo.2016.04.030
15. Fearon RE, Coop MR (2000) Reconstitution: what makes an appropriate reference material? Géotechnique 50(4):471–477. https://doi.org/10.1680/geot.2000.50.4.471
16. Ferrari A, Rosone M, Ziccarelli M, Giger SB (2020) The shear strength of Opalinus Clay shale in the remoulded state. Geomech Energy Environ 21:100142. https://doi.org/10.1016/j.gete.2019.100142
17. Gens A (2013) On the hydromechanical behavior of argillaceous hard soils-weak rocks. In: Proceedings of the 15th European Conference on Soil Mechanics and Geotechnical Engineering, pp 71–118. https://doi.org/10.3233/978-1-61499-199-1-71.
18. Gens A, Alonso EE (1992) A framework for the behaviour of unsaturated expansive clays. Can Geotech J. https://doi.org/10.1139/t92-120
19. Gonzalez-Blanco L, Romero E, Marschall P, Levasseur S (2022) Hydro mechanical response to gas transfer of deep argillaceous host rocks for radioactive waste disposal. Rock Mech Rock Eng 55:1159–1177. https://doi.org/10.1007/s00603-02102717-3
20. Huang Y, Zhu W, Qian X, Zhang N, Zhou Y (2011) Change of mechanical behavior between solidified and remolded solidified dredged materials. Eng Geol 3(4):112–119. https://doi.org/10.1016/j.enggeo.2011.03.005
21. Janbu N (1985) Soil models in offshore engineering. Geotech 35(3):241–281
22. Keller LM, Schuetz P, Erni R, Rossell MD, Lucas F, Gasser P, Holzer L (2013) Characterization of multi-scale microstructural features in Opalinus Clay. Microporous Mesoporous Mater 170:83–94
23. Khorshidi M, Lu N (2017) Intrinsic relationship between specific surface area and soil water retention. J Geotech Geoenviron Eng. https://doi.org/10.1061/(ASCE)GT.1943-5606.0001572
24. Kneuker T, Dohrmann R, Ufer K, Jaeggi D (2023) Compositional-structural characterization of the Opalinus Clay and Passwang Formation: new insights from Rietveld refinement (Mont Terri URL, Switzerland). Appl Clay Sci 242:107017. https://doi.org/10.1016/j.clay.2023.107017
25. Leupin OX, Bernier-Latmani R, Bagnoud A, Moors H, Leys N, Wouters K, Stroes-Gascoyne S (2017) Fifteen years of microbiological investigation in Opalinus Clay at the Mont Terri rock laboratory (Switzerland). Swiss J Geosci 110:343–354. https://doi.org/10.1007/s00015-016-0255-y
26. Lieske W, Baille W, Schmatz J, Kaufhold S, Dohrmann R (2021) Characterisation of natural and remoulded Onsøy clay with focus on the influence of mica. Eng Geol 295:106378. https://doi.org/10.1016/j.enggeo.2021.106378
27. Marschall P, Horseman S, Gimmi T (2005) Characterisation of gas transport properties of the Opalinus Clay, a potential host rock formation for radioactive waste disposal. Oil Gas Sci Technol 60(1):121–139. https://doi.org/10.2516/ogst:2005008
28. Meier L, Kahr G (1999) Determination of the cation exchange capacity (cec) of clay minerals using the complexes of copper(II) ion with triethylenetetramine and tetraethylenepentamine. Clays Clay Miner 47(3):386–388. https://doi.org/10.1346/CCMN.1999.0470315
29. Mitchell JK (1976) Fundamentals of soil behaviour, 1st edn. John Wiley & Sons, New York
30. Mitzscherling J, Genderjahn S, Schleicher AM, Bartholomäus A, Kallmeyer J, Wagner D (2023) Clay-associated microbial communities and their relevance for a nuclear waste repository in the Opalinus Clay rock formation. Microbiol Open 12:e1370. https://doi.org/10.1002/mbo3.1370
31. Neff KH (1959) Über die Messung der Wasseraufnahme ungleichförmiger bindiger anorganischer Bodenarten in einer neuen Ausführung des Enslingerätes. Bautechnik 39:415–421
32. Nitsch A, Leuthold J, Machacek J, Grandas Tavera CE (2023) Experimental investigations on hydro-mechanical processes in reconstituted clay shale and their significance for constitutive modelling. Rock Mech Rock Eng 40(3):405. https://doi.org/10.1007/s00603-022-03202-1
33. Romero E, Della Vecchia G, Jommi C (2011) An insight into the water retention properties of compacted clayey soils. Geotechnique 61(4):313–328. https://doi.org/10.1680/geot.2011.61.4.313
34. Romero E, Villar MV, Lloret A (2005) Thermo-hydro-mechanical behaviour of two heavily overconsolidated clays. Eng Geol 81(3):255–268. https://doi.org/10.1016/j.enggeo.2005.06.011

35. Rouf MA, Bouazza A, Singh RM, Gates WP, Rowe RK (2016) Water vapour adsorption and desorption in GCLs. Geosynth Int 23(2):86–99. https://doi.org/10.1680/jgein.15.00034
36. Schuster V, Rybacki E, Bonnelye A, Herrmann J, Schleicher A, Dresen G (2021) Experimental deformation of Opalinus clay at elevated temperature and pressure conditions: mechanical properties and the influence of rock fabric. Rock Mech Rock Eng 54:4009–4039. https://doi.org/10.1007/s00603-021-02474-3
37. Seiphoori A, Ferrari A, Laloui L (2014) Water retention behaviour and microstructural evolution of MX-80 bentonite during wetting and drying cycles. Géotechnique 64(9):721–734
38. Souza RFC, Pejon OJ (2020) Pore size distribution and swelling behavior of compacted bentonite/claystone and bentonite/sand mixtures. Eng Geol 275:105738. https://doi.org/10.1016/j.enggeo.2020.105738
39. Tang CS, Tang AM, Cui YJ, Delage P, Schroeder C, Shi B (2011) A study of the hydro-mechanical behaviour of compacted crushed argillite. Eng Geol 118(3–4):93–103. https://doi.org/10.1016/j.enggeo.2011.01.004
40. Ufer K, Kleeberg R, Bergmann J, Dohrmann R (2012) Rietveld refinement of disordered illite-smectite mixed-layer structures by a recursive algorithm. II: powder pattern refinement and quantitative phase analysis. Clays Clay Miner 60(5):535–552. https://doi.org/10.1346/CCMN.2012.0600508
41. Ufer K, Kleeberg R, Bergmann J, Dohrmann R (2012) Rietveld refinement of disordered Illite-smectite mixed-layer structures by a recursive algorithm. I: One dimensional patterns. Clays Clay Miner 60(5):507–534. https://doi.org/10.1346/CCMN.2012.0600507
42. Villar MV, Romero FJ, Martín PL, Gutiérrez-Rodrigo V, Barcala JM (2019) Experimental investigation of gas transport in the shaly facies of Opalinus Clay. In: Ferrari A, Laloui L (eds) Energy geotechnics. SEG 2018. Springer Series in Geomechanics and Geoengineering. Springer, Cham. https://doi.org/10.1007/978-3-319-99670-7_54
43. Wang H, Cui YJ, Vu MN, Zhang F, Talandier J (2023) On the hydro- mechanical behaviour of unsaturated damaged Callovo-Oxfordian claystone. Eng Geol 319:107107. https://doi.org/10.1016/j.enggeo.2023.107107
44. Wild KM, Amann F (2018) Experimental study of the hydro-mechanical response of Opalinus Clay – Part 2: influence of the stress path on the pore pressure response. Eng Geol 237:92–101. https://doi.org/10.1016/j.enggeo.2018.02.011
45. Wild KM, Amann F (2018) Experimental study of the hydro-mechanical response of Opalinus Clay – part 1: pore pressure response and effective geomechanical properties under consideration of confinement and anisotropy. Eng Geol 237:32–41. https://doi.org/10.1016/j.enggeo.2018.02.012
46. Wu F, Liu J, Liu T, Zhuang H, Yan C (2009) A method for assessment of excavation damaged zone (EDZ) of a rock mass and its application to a dam foundation case. Eng Geol 104(3–4):254–262. https://doi.org/10.1016/j.enggeo.2008.11.005
47. Zeng Z, Cui YJ, Talandier J (2021) Compaction and sealing properties of bentonite/claystone mixture: impacts of bentonite fraction, water content and dry density. Eng Geol 287:106122. https://doi.org/10.1016/j.enggeo.2021.106122
48. Zeng Z, Cui YJ, Talandier J (2023) Evaluation of swelling pressure of bentonite/claystone mixtures from pore size distribution. Acta Geotech 18:1671–1679. https://doi.org/10.1007/s11440-022-01676-5
49. Ziegler M, Brixel B, Lavasan AA, Christ F, Loew S (2022) Investigations in the new TBM-excavated Belchen highway tunnel: Summary and conclusions. ENSI Research and Experience 2021. (ENSI-AN-11284): 342–358
50. Ziegler M, Lukovic M, Lavasan AA, Christ F, Schoen M, Loew S (2021) Investigations in the new TBM-excavated Belchen highway tunnel - Status update (Part 5). ENSI Research and Experience 2020. (ENSI-AN-11061):313–320.